JOURNAL OF MATERIALS SCIENCE 20 (1985) 4169–4184

The fracture of hybrid-particulate composites

A. J. KINLOCH
Department of Mechanical Engineering, Imperial College of Science and Technology, Exhibition Road, London SW7 2BX, UK

D. L. MAXWELL, R. J. YOUNG
Department of Materials, Queen Mary College, Mile End Road, London E1 4NS, UK

The fracture behaviour of hybrid-particulate composites has been examined. These novel materials contain both dispersed rubbery and rigid glass particles, and values of the stress-intensity factor K_{Ic} and fracture energy G_{Ic} have been determined using a double-torsion test. Considerable increases in toughness have been recorded and the mechanisms of toughening have been identified. The rigid glass particles increase the crack resistance mainly through a crack-pinning mechanism whilst the rubbery particles, which have a much greater effect, enhance the extent of localized plastic shear deformations around the crack tip. Quantitative failure theories and criteria are suggested for these mechanisms.

1. Introduction

Epoxy polymers are widely employed as the basis for adhesive compositions and as the matrix material for composites containing glass, polyamide and carbon fibre. When cured, epoxy resins are highly crosslinked, amorphous thermoset polymers. This structure results in these polymers possessing many useful engineering properties, such as a relatively high modulus and strength, good creep resistance and good elevated-temperature properties. However, it also means that unmodified expoxies are relatively brittle polymers with poor resistance to crack propagation.

To increase the crack resistance, but without seriously impairing other important properties, two methods have been reported [1] based upon attaining a dispersion of a particulate second phase in the epoxy. In one method the second-phase is rubbery in character [2–6] whilst in the other it consists of rigid brittle particles such as alumina, silica and glass spheres [7–11].

As might be expected, the mechanisms of deformation and fracture are notably different in the two cases, and in an effort to attain the optimum properties from toughened epoxy polymers we have been investigating the structure/property relationships of hybrid-particulate composites. These novel materials contain both rubbery and rigid dispersed phases. A separate paper [12] has considered the relationship between the microstructure of such composites and the measured modulus and yield behaviour. The present paper is concerned with the fracture properties of hybrid-particulate composites and considers toughening mechanisms and failure criteria.

2. Experimental details

2.1. Materials

The epoxy resin employed was derived from the reaction of bisphenol A and epichlorhydrin, and was largely composed of the diglycidyl ether of bisphenol A (DGEBA), but small quantities of higher molar-mass polymers were present. The curing agent was piperidine.

0022–2461/85 $03.00 + .12

The rubber used was a carboxyl-terminated, random copolymer of butadiene and acrylonitrile, CTBN (carboxyl content: 2.37 wt %; acrylonitrile content: 18 wt %; molar mass: 3500 g mol^{-1}).

The rigid particulate filler was glass beads with a distribution of particle diameters from about 10 to 100 μm and an average diameter of 50.3 μm. In some instances the glass beads were coated with a reactive silane-based bonding agent. This was γ-glycidoxypropyltrimethoxysilane, which was applied by immersing the glass beads for 30 min in a 1 vol % solution of ethanol : water (95 : 5 by volume) and then drying the glass beads for 1 h at room temperature, 4 h at 40° C and finally 1 h at 120° C. Three types of composites were fabricated: epoxy/glass, epoxy/glass/rubber and epoxy/glass (silane)/rubber, and details of the nominal compositions are given in Table I.

Sheets of the hybrid-particulate composites (i.e. containing both rubber and glass beads) were prepared by first adding the CTBN rubber to the DGEBA resin and hand-mixing for ~ 5 to 10 min. This mixture was then heated to 65 ± 5° C in a water bath and mixed for 5 min using an electric stirrer. The resin mixture was next degassed in a vacuum oven at 60° C until frothing stopped, i.e. most of the entrapped air had been removed. When the mixture had cooled to below 30° C the piperidine curing agent was mixed in gently to minimize air entrapment. The mixture was re-heated to 65° C and the glass beads were now gently stirred into the mixture which was then allowed to stand at 120° C for 15 to 100 min (depending upon the glass content) to increase the viscosity of the system just sufficiently to prevent the glass beads from settling out during moulding. Prior to casting the glass-filled systems were again gently stirred. The resin mixture was then poured into a preheated mould and cured at 120° C. The total time allowed for curing at 120° C was 16 h, which in the case of glass-filled composites included the standing time at 120° C. The cured sheet of epoxy composite was allowed to cool slowly, in the mould, to room temperature. The epoxy polymers containing no rubber and/or no glass beads were prepared in the same manner, but obviously the rubber addition and/or the glass-bead addition steps were omitted.

TABLE I Formulations of epoxy polymers

Component	Composition (phr)*
Epoxy resin	100
Piperidine	5
CTBN	0 or 15
Glass beads†	0, 10, 23, 35, 50, 100, 200 or 300

*phr = Parts per hundred of resin by weight.
†Used either uncoated or coated with a silane-based bonding agent (see Section 2.1).

To ensure that the presence of the glass particles did not interfere with the formation of the rubbery second phase, the glass transition temperatures T_g of the hybrid-particulate composites were determined. Differential scanning calorimetry was employed using a Perkin–Elmer Model 1B and a heating rate of 20 K min^{-1}. The value of the T_g was 95 ± 2° C for all the materials, indicating that the presence of glass particles in the hybrid-particulate composites did not affect the extent of phase separation of the rubber. The exact volume fractions of glass were checked by burning off the resin and weighing the residues.

2.2. Crack-propagation studies

Crack propagation in the various epoxy composites was investigated using the double torsion (DT) test, which gave good control of the propagating crack and enabled the easy and rapid determination of the critical stress-intensity factor K_{Ic}. The technique has been described in detail elsewhere [1, 13] and it may be shown that K_{Ic} is independent of crack length, and for a linear-elastic material given approximately [8] by

$$K_{Ic} = P_c l_m \left[\frac{(1 + \nu)}{l b^3 b_n k}\right]^{1/2} \quad (1)$$

where P_c is the critical load for crack propagation, l_m is the moment arm, ν the Poisson's ratio of the material ($\nu = 0.35$), l the width of the specimen, b the sheet thickness, b_n the sheet thickness in the plane of the crack and k a geometry constant (taken to be 0.249).

The 6 mm thick moulded epoxy sheets were cut into rectangular plates 80 mm long and 30 mm wide. They were notched at one end with a sharp razor blade and a V-shaped groove, 2.0 mm deep, was machined along the centre of one face. The specimens were then deformed in the DT rig [1, 8] in an Instron Universal testing machine over a range of test temperatures from − 70° to + 50° C at a constant cross-head speed

of 0.5 mm min^{-1}. The value of K_{Ic} was determined from Equation 1 using the measured value of P_c and knowing the specimen dimensions. No attempt was made to measure the crack velocity.

The fracture energy G_{Ic} may be related [1, 13] to the stress-intensity factor, K_{Ic}, by the equation

$$G_{Ic} \sim K_{Ic}^2/E \quad (2)$$

where E is the Young's modulus. Values of E for the epoxy composites were reported in a previous publication [12], and thus values of G_{Ic} may be deduced for Equation 2.

2.3. Fractography

The fracture surfaces of a large number of specimens were examined using both optical and scanning electron microscopy. Before observation in the scanning electron microscope the specimens were sputter-coated with a thin layer ($\sim$ 20 nm) of platinum to make the surfaces conductive and reduce charging.

3. Results and discussion

3.1. Stability of crack propagation

3.1.1. Types of crack propagation

It has been shown [1, 5, 14] that, depending upon the test conditions and the composition of the material, three distinct types of crack propagation may be observed in thermosetting epoxy polymers. These are:

1. Stable brittle propagation (Type C). Here the crack grows in a steady controlled manner with the rate of crack propagation being dependent upon the cross-head speed of the testing machine. The fracture surfaces of the unmodified resin are relatively featureless and, since cracks grow at low levels of K_{Ic} (typically about 1 MN m$^{-3/2}$), stable brittle propagation may be thought of as a classic example of brittle fracture. The associated load–displacement curve for the DT specimen is shown schematically in Fig. 1a and, as may be seen, the crack propagates at a constant load.

2. Unstable brittle propagation (Type B). This type of crack growth is still essentially brittle in nature, but the crack propagates intermittently in a stick/slip manner. This type of crack growth has a significant effect on the associated load–displacement curve which now has a characteristic sawtooth shape (Fig. 1b). The values of P_i and P_a correspond to loads at crack initiation and arrest respectively. The initiation and arrest values of K_{Ic} and G_{Ic} may be determined from P_i and P_a through Equations 1 and 2.

3. Stable ductile propagation (Type A). Again the crack grows steadily in a controlled manner, and for the DT specimen the load for crack propagation is constant as in Fig. 1a. However, unlike the stable brittle propagation discussed in (1) a relatively high value of K_{Ic} is now required and the fracture surfaces are far rougher and torn in appearance, indicating a more ductile fracture process.

Now these three basic types of crack propagation behaviour are all observed in the epoxy composites studied in the present investigation and, as for the unfilled epoxy polymers, the exact type observed is dependent upon the test conditions (i.e. test temperature in the present work) and the detailed composition of the material.

3.1.2. Effect of test temperature

The typical effect of test temperature upon the crack growth behaviour and associated value of K_{Ic} is illustrated in Fig. 2 for a hybrid particulate composite (rubber = 15 phr; v_f(glass (silane)) = 0.085). At the highest temperatures, stable ductile crack growth (Type A) is observed and as the temperature is decreased the value of K_{Ic} steadily decreases. At about 0° C the mode of crack

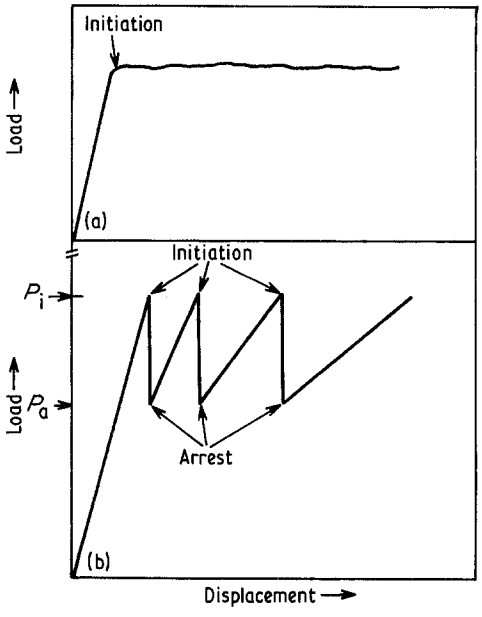

Figure 1 Typical schematic load against displacement curves for the epoxy composites: (a) continuous, stable propagation; (b) unstable, stick/slip propagation.

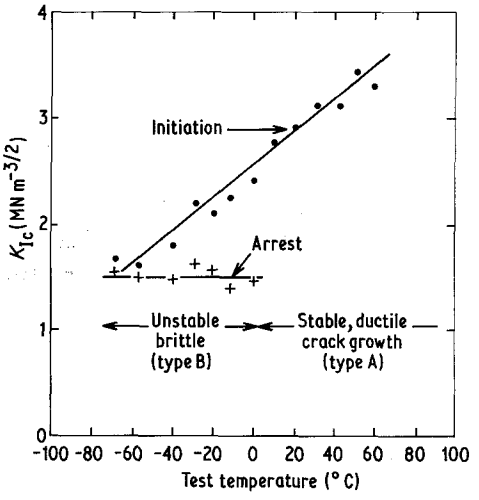

Figure 2 Stress-intensity factor K_{Ic} for crack propagation, and observed modes of crack growth, as a function of test temperature for a hybrid-particulate composite (rubber = 15 phr; v_f(glass (silane) = 0.085).

propagation changes to unstable brittle (Type B), and initiation and arrest values of K_{Ic} may be deduced. The former continues to decrease as the temperature is further lowered but the arrest value is virtually independent of temperature, again in accord with previous work [14]. Stable brittle crack growth (Type C) is rarely observed in the hybrid particulate composites (i.e. those containing both rubber and glass particles) but is observed regularly in the unfilled and glass-filled materials. However, in all cases it is only observed at the very lowest temperatures.

The increase in K_{Ic} with increasing temperature and the observed transitions in the crack propagation behaviour (Type C to Type A as the temperature increases) have been previously recorded [1, 5] for both unfilled and rubbery-particulate filled epoxies, and have been ascribed to crack-tip blunting. This mechanism will be considered in more detail later but essentially it proposes [1, 13, 15, 16] that the above observations are a result of the localized plastic deformations that occur in the vicinity the crack tip. Such deformations increase with increasing temperature and so cause progressive crack-tip blunting. Therefore at low temperatures, when the yield stress is high (see Fig. 4 in Young *et al.* [12]), a relatively sharp crack results and the value of K_{Ic} is low and stable; brittle crack propagation is observed. At somewhat higher temperatures the yield stress is lower and crack-tip blunting occurs. This results in higher loads for crack initiation (i.e. higher K_{Ic}(initiation) values) but, when the crack does eventually propagate the rate of release of energy is now greater than that required for stable crack growth and hence unstable propagation is observed. At even higher temperatures the degree of crack-tip blunting is so severe that a ductile or tearing type of failure mode is achieved and stable crack growth is observed once again, but now associated with a relatively high K_{Ic} value. This mechanism obviously qualitatively explains the results illustrated in Fig. 2.

3.1.3. Effect of composition

The general crack propagation behaviour described above is a characteristic of all the com-

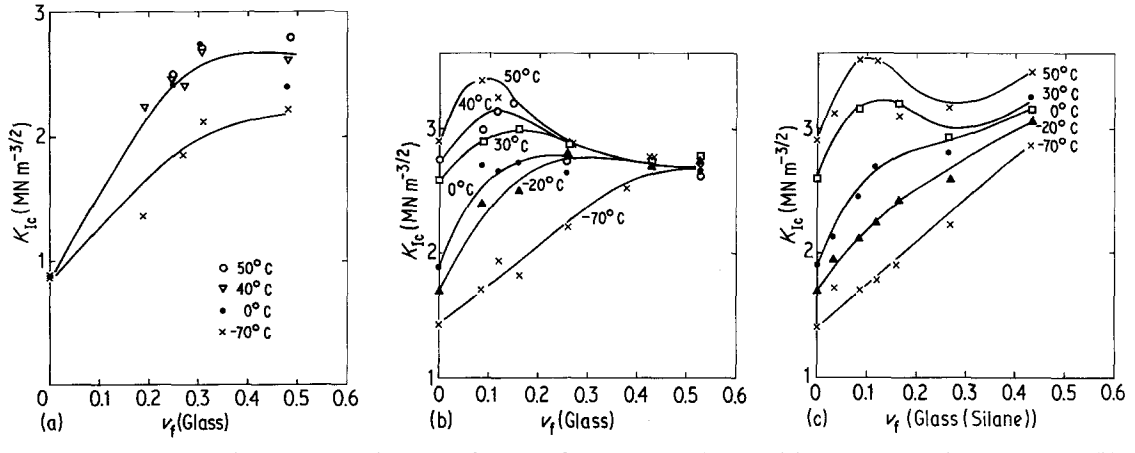

Figure 3 Stress-intensity factor K_{Ic} as a function of volume fraction v_f of glass particles: (a) epoxy–glass composite; (b) hybrid-particulate composite (i.e. epoxy–glass–rubber (15phr)); (c) hybrid-particulate composite containing silane-coated glass particles. (Note that the ordinate only starts at K_{Ic} = 0 for (a).)

positions examined. However, the temperatures at which the transitions in the type of crack growth occur are a function of composition. The main effect is that the presence of rubber particles lowers the temperature for the transitions from Type C to Type B and Type B to Type A, as previously observed [5, 6] for non-glass-filled epoxies. The same effect, although to a lesser extent, is generally produced if the volume fraction v_f of glass is increased in a given system; an exception occurs for the epoxy–glass–rubber composites at the highest values of v_f(glass) when large-scale debonding of the glass particles is observed, as shown later. The reductions in the transition temperatures that result from the presence of rubber and glass particles arise from the particles inducing more energy losses around the crack tip, and the mechanisms involved will be considered later.

3.2. Stress-intensity factor

The measured values of the stress-intensity factor K_{Ic} at the onset of crack propagation are shown as a function of the volume fraction v_f of glass particles for various test temperatures in Fig. 3.

The data for the epoxy–glass composite are shown in Fig. 3a. The initial increase in K_{Ic} with increasing volume fraction of glass, but with K_{Ic} reaching a plateau value at high values of v_f(glass), is in accord with previous observations [10].

The data for the hybrid composites are shown in Fig. 3b (epoxy–glass–rubber (15 phr)) and Fig. 3c (epoxy–glass (silane)–rubber (15 phr)), and similar effects are observed for both materials. At temperatures below about 0° C the K_{Ic} against v_f(glass) relations follow the same trend as described above, but with the K_{Ic} values being appreciably higher due to the presence of the rubber particles. However, at higher temperatures a maximum in K_{Ic} is observed which becomes more pronounced as the temperature is increased. The maximum in K_{Ic} occurs at a v_f(glass) value of about 0.1. These observations of a peak in the K_{Ic} against v_f(glass) relations represent the first instance such an effect has been recorded for glass-filled epoxy polymers. It undoubtedly arises from the relatively high K_{Ic} values for the hybrid composites, and hence the high crack-tip stresses which act upon the glass particles. This will be discussed later when the fracture mechanisms are considered.

3.3. Fracture energy

The fracture energy G_{Ic} was calculated using Equation 2 together with the values of K_{Ic} and E measured previously. Values of G_{Ic} as a function of v_f(glass) for various test temperatures are shown in Fig. 4.

Considering first the epoxy–glass composite (Fig. 4a), then the value of G_{Ic} passes through a maximum at a v_f(glass) value of about 0.25. This is in direct contrast to the K_{Ic} data for this composite (Fig. 3a) where K_{Ic} increased steadily to a plateau value. As discussed in detail by Spanoudakis and Young [10, 11], this maximum in G_{Ic} essentially arises from the different dependencies of K_{Ic} and E upon v_f(glass) and no change in failure mechanism, for example, is necessarily associated with the peak.

Considering the hybrid composites (Figs. 4b and c), then the G_{Ic} against v_f(glass) data again exhibit peaks. However, in comparison to the

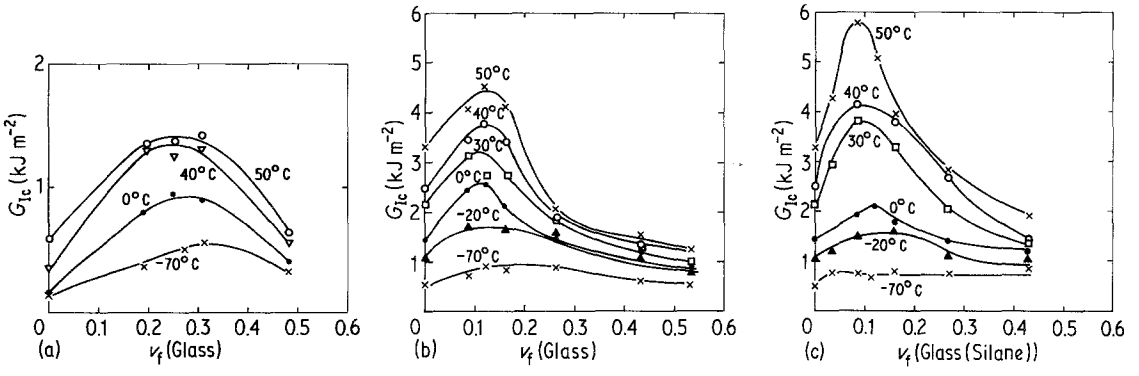

Figure 4 Fracture energy G_{Ic} as a function of volume fraction v_f of glass particles: (a) epoxy/glass composite; (b) hybrid-particulate composite; (c) hybrid-particulate composite containing silane-coated glass particles. (Note the different scale for the ordinate in (a).)

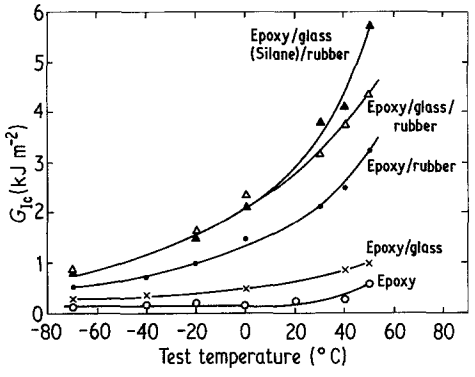

Figure 5 Fracture energy G_{Ic} against test temperature for all the materials studied (where appropriate v_f(glass) = 0.1).

epoxy–glass composite (Fig. 4a) the peaks are far more pronounced, particularly at high temperatures, and occur at a v_f(glass) of about 0.1. Obviously, the position and shape of these peaks largely arise from the peaks observed in the K_{Ic} data for the hybrid composites (Figs. 3b and c) but are magnified by E increasing as the v_f(glass) is increased (see Fig. 1 in Young *et al.* [12]).

Values of G_{Ic} for all the materials studied are shown in Fig. 5 as a function of test temperature. For the glass-filled materials a v_f(glass) of 0.1 has been selected since for the hybrid-particulate composites this represents the volume fraction of glass at which the fracture energy is approximately at its maximum value. As may be seen, there is a significant increase in G_{Ic} for the glass-filled composites compared to the respective non-glass-filled materials over the complete temperature range. It is especially noteworthy that this is the case for the hybrid-particulate composites. Hence, the addition of a relatively *low* volume fraction of glass particles has substantially improved the fracture resistance of an epoxy polymer, which has already been appreciably toughened due to the presence of rubber particles. Further, in some hybrid-particulate composites a silane bonding agent was coated on to the glass particles to increase the interfacial adhesion. However, as may be seen, such materials only possess higher fracture energies compared to the uncoated-glass hybrid composites at the highest temperatures; again the underlying reasons for this observation will be considered when the mechanisms of toughening are discussed.

One aim when attempting to toughen brittle polymers is to increase the toughness without significantly decreasing other important properties, such as modulus. The data in Table II again clearly demonstrate the major increases in G_{Ic} attained for the hybrid composites (v_f(glass) = 0.1) without any significant decreases in the values of E.

4. Mechanisms of toughening

The results discussed in the previous section demonstrate that the fracture toughness K_{Ic} and fracture energy G_{Ic} of both simple epoxy and rubber-toughened epoxy polymers are greatly increased by the inclusion of a glass-particulate filler. In the present section the mechanisms responsible for the increased crack resistance will be proposed and discussed.

4.1. Crack pinning

4.1.1. Introduction

In 1971 Lange and Radford [7] reported that the fracture energy of an epoxy thermosetting polymer could be significantly increased by the inclusion of a rigid particulate filler (alumina trihydrate) and suggested that a crack-pinning mechanism was responsible. The crack-pinning mechanism had been proposed earlier by Lange [17] and has since been modified and extended by Evans [18] and Green *et al.* [19, 20]. Basically, it assumes that cracks can be impeded by rigid, impenetrable, well-bonded particles. This arises

TABLE II Comparison of modulus and fracture-energy values

	−70° C		+50° C	
	E (GPa)	G_{Ic} (kJ m^{-2})	E (GPa)	G_{Ic} (kJ m^{-2})
Epoxy	4.1	0.15	2.8	0.50
Epoxy–glass*	4.3	0.26	3.1	1.0
Epoxy–rubber†	3.3	0.60	2.2	3.3
Hybrid†	4.1	0.80	2.6	4.3
Hybrid‡ (using silane-treated glass particles)	4.3	0.75	2.5	5.8

*v_f(glass) = 0.1; †rubber = 15 phr; ‡v_f(glass) = 0.1, rubber = 15 phr.

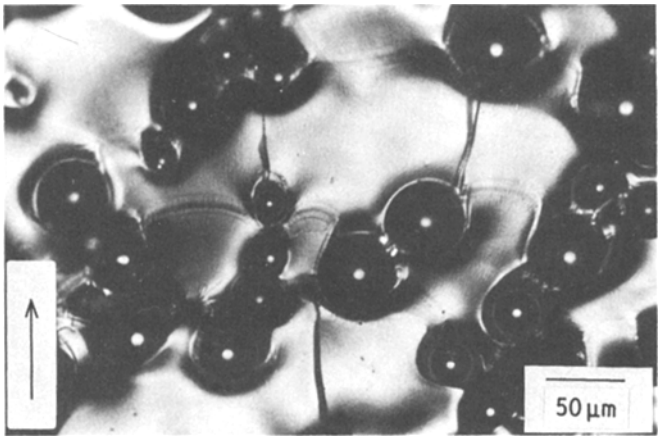

Figure 6 Optical micrograph of glass-filled epoxy composite showing the pinned crack-front bowing between glass particles. (Arrow indicates direction of crack propagation.)

since when a crack meets an array of such obstacles it becomes pinned and tends to bow out between the particles, forming secondary cracks. Thus new fracture surface is formed and the length of the crack front is increased due to its change of shape between the pinning positions. Now energy is not only required to create the new fracture surface but, by analogy with the theory of dislocations, energy must also be supplied to the newly formed non-linear crack front, which is assumed to possess a line energy. This latter factor particularly is suggested to lead to the enhanced crack resistance often observed when impenetrable particles are well bonded into a brittle matrix.

The fractographic studies provide strong evidence that crack pinning is an operative mechanism in the glass-particulate composites. Fig. 6 clearly shows crack bowing between glass particles, and also suggests that the pinned crack assumes an elliptical shape at breakaway. Further, when such secondary cracks do eventually break away from the pinning positions then this frequently leads to characteristic tails or steps on the fracture surface at the rear of the inclusions, due to the meeting of the two arms of the crack front from different fracture planes. The scanning electron micrographs shown in Fig. 7 illustrate these features for an epoxy/glass ($v_f = 0.19$) and untreated and silane-treated hybrid-particulate composites ($v_f(\text{glass}) = 0.12$). For the hybrid-particulate composite the dispersed rubber particles, having a diameter of about 1 to 3 μm, may be clearly distinguished. However, these rubber particles induce more localized plastic deformations around the crack, leading to a somewhat rougher fracture surface. Notwithstanding this, the presence of tails or steps behind the glass particles may still be discerned. Another interesting difference between the fracture surfaces shown in Fig. 7 is that the cracks propagating through the composites appear to be attracted to the equators of the particles for the glass-filled epoxy (Fig. 7a) and the hybrid-particulate composite (Fig. 7b), but more towards the poles of the particles in the hybrid-particulate composite containing silane-coated glass (Fig. 7c). This can be explained by considering the local stresses around the rigid glass particles in an epoxy resin under an applied stress. As the interfacial adhesion between the particle and matrix is increased then the maximum tensile stress moves from the equatorial regions to the poles of the particles [21–23]. Thus, propagating cracks will be attracted to the equatorial regions of the particles when the interfacial adhesion is relatively low but towards the poles when it is higher, due for example to the use of a reactive silane-bonding agent. Finally, micrographs shown in Fig. 7 represent typical micrographs for low and moderate volume fractions of glass. At high volume fractions, tails or steps were rarely observed but, as commented previously [10, 11], the absence of such features does not necessarily mean that no pinning occurs. For example, such features will be obscured at high volume fractions due to the considerable overlap of secondary cracks. Also, at higher volume fractions the interacting stress fields may lead to premature debonding of the particles, and debonded particles are not effective pinning sites.

4.1.2. Theory

In the original work by Lange [17] an expression was derived relating the fracture energy G_{Ic} of

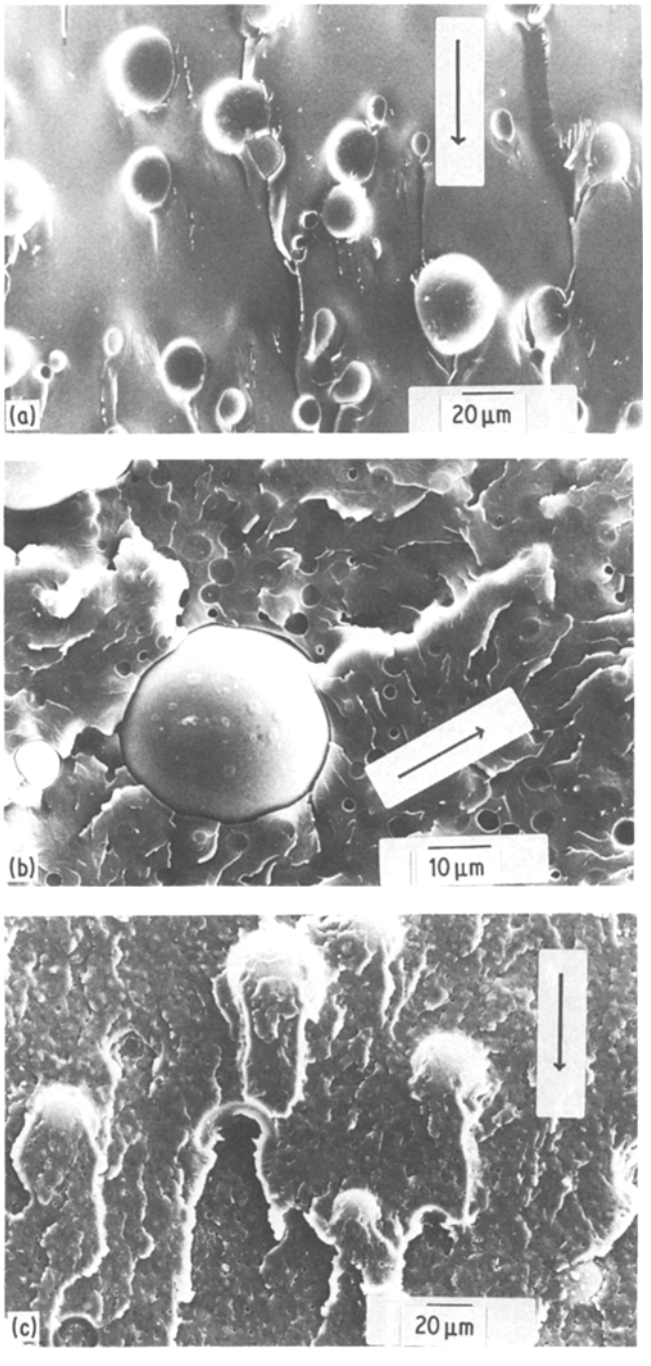

Figure 7 Scanning electron micrographs of fracture surfaces: (a) epoxy–glass (v_f(glass) = 0.19) composite, test temperature = −70° C; (b) hybrid-particulate composite (v_f(glass) = 0.12), test temperature = 30° C; (c) hybrid-particulate composite containing silane-coated glass particles (v_f(glass (silane)) = 0.12), test temperature = −70° C. (Arrows indicate direction of crack propagation.)

the composite to that of the matrix, G_{Ic}(matrix), through the line energy T_L per unit length of bowed crack front. By assuming that the crack front breaks away from the pinning positions when it attains a radius of $D_s/2$, where D_s is the interparticle spacing, Lange obtained the relation

$$G_{Ic} = G_{Ic}(\text{matrix}) + 2T_L/D_s \quad (3)$$

However, this equation has been found [1, 7, 9, 10] to be inadequate to describe the crack-pinning mechanism. For example, the initial slopes of plots of G_{Ic} against D_s^{-1} are often a function of the volume fraction of glass, and thus the value of T_L is not invariant with particle size as suggested by Equation 3.

More satisfactory theoretical models have been derived by several groups of workers [18,

TABLE III Predicted values of σ_c/σ_m as a function of d_p/D_s for particle-filled composites

d_p/D_s	Non-interacting elliptical cracks		Interacting elliptical cracks	
	Evans [18]	Green *et al.* [20]	Evans [18]	Green *et al.* [20]
0	1.00	1.00	1.00	1.00
0.25	1.85	2.02	1.19	1.19
0.50	2.18	2.52	1.65	1.80
1.00	2.55	3.05	2.23	2.52
1.25	2.70	3.25	2.40	2.86
2.00	2.90	3.75	2.75	3.52

20] who have calculated from first principles the stresses required to propagate a crack through a matrix reinforced by an array of rigid particles. This was first undertaken by Evans [18] who demonstrated that the line-energy contribution is a major mechanism for rigid, impenetrable particles but that the value of T_L is indeed a function of particle size and shape. Evans' analysis also enables the fracture strength of particulate composites to be predicted. The results are given in Table III where the ratio of the stress required to propagate a crack in the composite to the stress required for a crack in pure matrix, σ_c/σ_m, is given in terms of the ratio of the particle diameter to the interparticle separation, d_p/D_s. Values are given for elliptical secondary crack fronts and for both the assumptions of (i) no interactions between elliptical secondary cracks and (ii) crack interactions. Green *et al.* [20] have modified the Evans' analysis and, in particular, have taken into account the exact position of the secondary crack front when it breaks away from the pinning positions. They obtained a similar dependence of σ_c/σ_m with d_p/D_s as Evans, as may be seen from Table III, but their analysis yields somewhat higher values of σ_c/σ_m. For a particulate composite and an unfilled polymer containing primary cracks of the same length then the ratio σ_c/σ_m is equivalent to the ratio K_{Ic}(composite)/K_{Ic}(matrix).

From the above discussions and those in Section 3 it is already clear that the fracture of glass-filled epoxy polymers, especially of the hybrid-particulate composites, is complex with several toughening mechanisms operating. Therefore to ascertain whether the quantitative predictions of Evans [18] and Green *et al.* [20] adequately describe the contribution of crack pinning it is necessary to select values of K_{Ic} when contributions from other mechanisms are likely to be least important. Since crack-tip blunting arising from plastic deformation of the epoxy has already been identified as a main mechanism, then this implies that values of K_{Ic} at low temperatures, when the crack tip is relatively sharp, are the most appropriate. Thus values of the stress-intensity factor were deduced at low temperatures by either taking the value of the intersection of the initiation and arrest values (see Fig. 2) or, if stable growth had occurred, by taking the value at $-70°$ C, i.e. the lowest temperature employed.

Measured values of the ratio K_{Ics}(glass-filled)/K_{Ics}(unfilled) are plotted against the ratio d_p/D_s in Fig. 8, where the values of d_p/D_s were calculated from

$$\frac{d_p}{D_s} = \frac{3v_f}{2(1 - v_f)} \quad (4)$$

The solid lines represent the theoretical expressions of Evans [18] and Green *et al.* [20] for interacting elliptical secondary cracks. As may

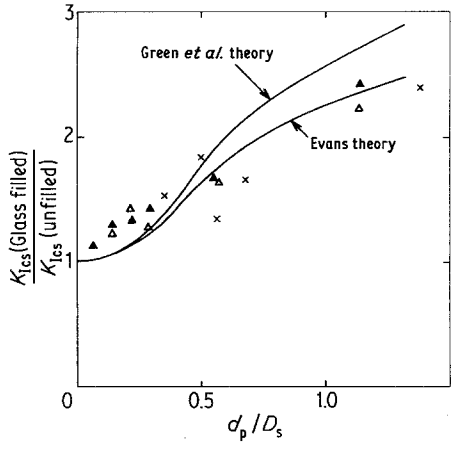

Figure 8 Variation of K_{Ics}(glass-filled)/K_{Ics}(unfilled) with d_p/D_s for the various composites. The solid lines are the theoretical predictions of Evans [18] and Green *et al.* [20] for interacting elliptical cracks. (×) Epoxy–glass, (△) epoxy–glass–rubber, (▲) epoxy–glass (silane)–rubber.

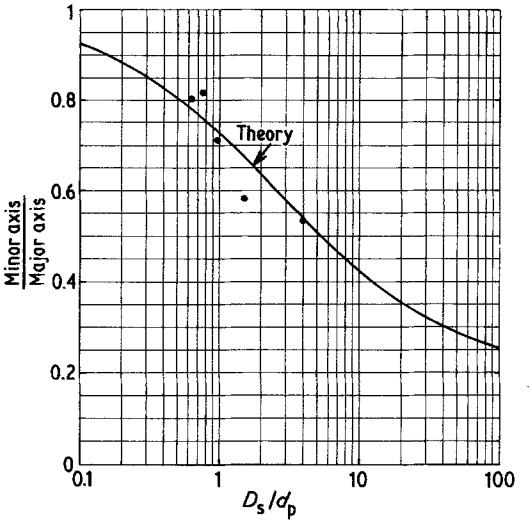

Figure 9 Shape of the pinned crack front at breakway as a function of (interparticle separation)/(particle diameter), (D_s/d_p). Points experimental; solid curve theoretical.

be seen, the agreement between theory and experiment is good, with the three different composite systems following the theoretical predictions quite closely. In contrast, if the effect of plastic deformations around the crack tip causing blunting had not been taken into account then the agreement would not have been so good.

Finally, the theoretical work of Evans [18] and Green *et al.* [20] also enables the shape of the pinned crack front at breakaway to be calculated as a function of the ratio of the interparticle separation to the particle diameter (D_s/d_p). The results of the calculations are shown in Fig. 9 and indicate that for high volume fractions of glass the crack shape at breakaway (defined by the ratio of the length of the minor axis of the elliptical crack to that of the major axis) tends to be semicircular, whilst for low volume fractions the crack front tends to remain straight. The experimental measurements of the crack shape at breakaway for various D_s/d_p values were taken from optical micrographs, such as that shown in Fig. 6, and are in good agreement with the theoretical calculations, as may be seen from Fig. 9. This again confirms the role of the crack-pinning mechanism and the general agreement with the model advanced by Evans [18] and extended by Green *et al.* [20].

4.1.3. Interfacial adhesion

Weak interfacial adhesion between the rigid particles and the matrix impairs the efficiency of the crack-pinning mechanism, since if particles become debonded they are ineffectual as pinning positions [19]. To improve the interfacial adhesion of the glass particles in the hybrid-particulate composites the particles were coated with a silane bonding agent (γ-glycidoxypropyltrimethoxy silane) which has been shown [24] to increase the interfacial adhesion between glass and epoxy resins. As may be seen from Figs. 3, 4 and 5 and Table II, the main effect is to increase the fracture resistance of the hybrid-particulate composites at the highest test temperatures. Under these conditions the stress field at the crack tip acting upon the particles is very high, and particle debonding is therefore likely to occur and to impair the crack-pinning mechanism. Evidence for the improved interfacial adhesion obtained when using the silane-coated glass particles is shown in Fig. 10. The scanning electron micrograph of the fracture surface of the hybrid-particulate composite containing silane-coated particles (Fig. 10b) reveals that the glass particles are more firmly bonded to the matrix polymer. Indeed, in some instances a layer of material containing rubber particles is clearly still bonded to the glass particle. Thus, the improved adhesion resulting from employing the silane bonding agent appears to inhibit debonding at the highest test temperatures and so increases the efficiency of the crack pinning mechanism, thereby increasing the values of K_{Ic} and G_{Ic} for the hybrid-particulate composites under these conditions.

Turning to the reasons for the maxima in the K_{Ic} against v_f(glass) relations for the hybrid-particulate composite (Figs. 3b and c), then particle debonding is again a possible cause. As stated above, the high K_{Ic} values at the higher test temperatures for the hybrid composites cause the glass particles ahead of the crack tip to be subjected to high stresses. At high volume fractions this will be amplified by interactions between the stress fields around particles, and could lead to particle debonding and a reduction in the contribution from crack pinning. This effect would be expected to be less for the silane-coated hybrid composites and, indeed, the maxima in the K_{Ic} peaks are less pronounced for this material (see Figs. 3b and c).

4.1.4. Failure criterion

Crack propagation in many glassy thermo-

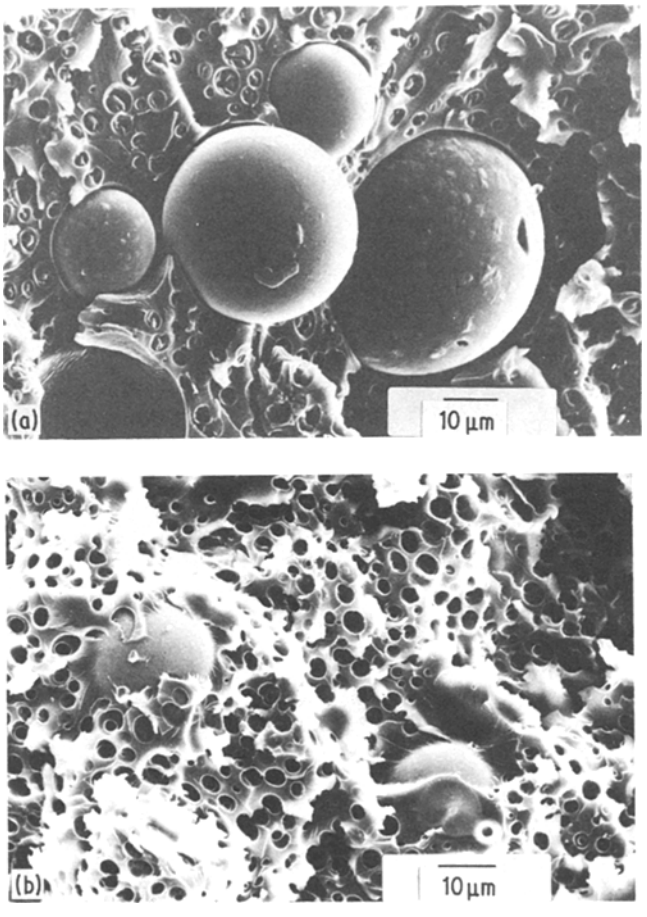

Figure 10 Scanning electron micrographs of fracture surfaces: (a) hybrid-particulate composite containing uncoated particles; (b) hybrid-particulate composite containing silane-coated glass particles. (v_f of glass = 0.085; test temperature 50° C.)

plastic polymers is controlled by a critical crack-opening displacement criterion [1, 13]. It has also been shown that stable brittle crack propagation in thermosetting epoxy polymers is governed, to a first approximation, by this criterion until crack-tip blunting occurs and causes unstable propagation [6, 14].

Thus, for the particulate composites the relevant value of the crack-opening displacement δ_{tc} is given by

$$\delta_{tc} = \frac{K_{Ics}^2}{E\sigma_{yt}} \quad (5)$$

where σ_{yt} is the tensile yield stress. The value of K_{Ics} was deduced as described above, and the values of E and the compressive yield stress σ_{yc} at the corresponding temperature were taken from previous work [12]; the corresponding value of σ_{yt} was calculated assuming $\sigma_{yt}/\sigma_{yc} = 0.75$ as discussed previously [25].

In order to examine the validity of a constant δ_{tc} criterion for the particulate composites, K_{Ics} is plotted against $(E\sigma_{yt})^{1/2}$ in Fig. 11. As may be seen, linear relationships are obtained for both the glass-filled simple epoxy composite and the hybrid-particulate composites which yield values of δ_{tc} of 1.8 and 4.4 μm respectively. Thus, when crack pinning is a main mechanism the onset of

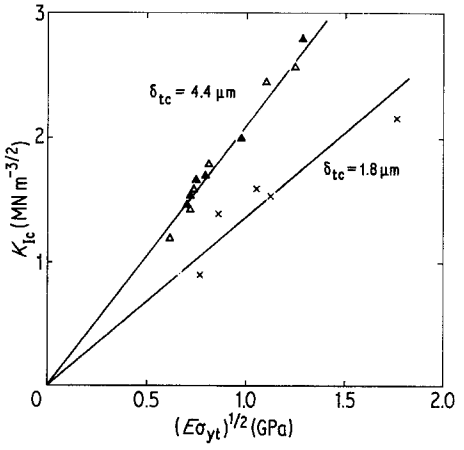

Figure 11 Variation of K_{Ics} with $(E\sigma_{yt})^{1/2}$ for the various composites: (×) epoxy–glass, (△) epoxy–glass–rubber, (▲) epoxy–glass(silane)–rubber.

crack propagation may be described by a constant crack-opening displacement.

4.2. Localized plastic deformations

4.2.1. Introduction

Many different mechanisms have been proposed [1] to explain the greatly improved toughness that may result when a thermosetting polymer possesses a multiphase microstructure of dispersed rubber particles. The recent mechanism proposed by Kinloch and co-workers [5, 6] best explains the experimental evidence and has received independent verification from the work of Yee and Pearson [26].

This mechanism proposed that the greater fracture resistance in the rubber-modified thermosetting polymers arises from a greater extent of energy-dissipating deformations occurring in the material in the vicinity of the crack tip. The deformation processes are (1) cavitation in the rubber, or at the particle/matrix interface, and (2) multiple but localized plastic-shear yielding in the matrix, initiated by the rubber particles. The localized cavitation of the rubber gives rise to the stress-whitening that often accompanies crack growth, especially at high temperatures, and is observed in the hybrid-particulate composites. Indeed, this cavitation of the rubber particles is also strikingly apparent in the scanning electron micrograph shown in Figs. 10 and 12a, where the rubber particles appear as partially-filled holes following the cavitation mechanism [5]. However, localized plastic-shear yielding is the main source of energy dissipation and increased toughness. It occurs to a far greater extent in the epoxy matrix of the rubber-modified polymers, compared to the simple epoxy polymer, due to interactions between the stress field ahead of the crack and the rubber particles [5, 6]. This is evident by comparing Figs. 12a and b, which show fracture surfaces from tests conducted at 30° C. There is little sign of plastic deformation in the matrix of the glass-filled simple epoxy composites (Fig. 12b), whilst there is considerable deformation in that of the hybrid-particulate composite (Fig. 12a), with

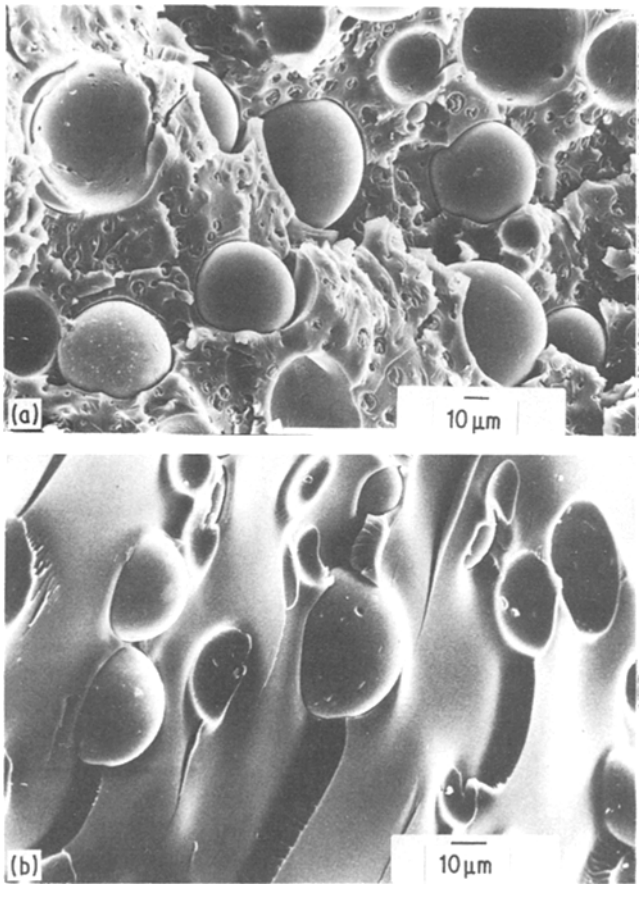

Figure 12 Scanning electron micrograph of fracture surfaces: (a) hybrid-particulate composite (v_f(glass) = 0.12); (b) glass-filled simple epoxy composite (v_f(glass) = 0.19). (Test temperature = 30° C.)

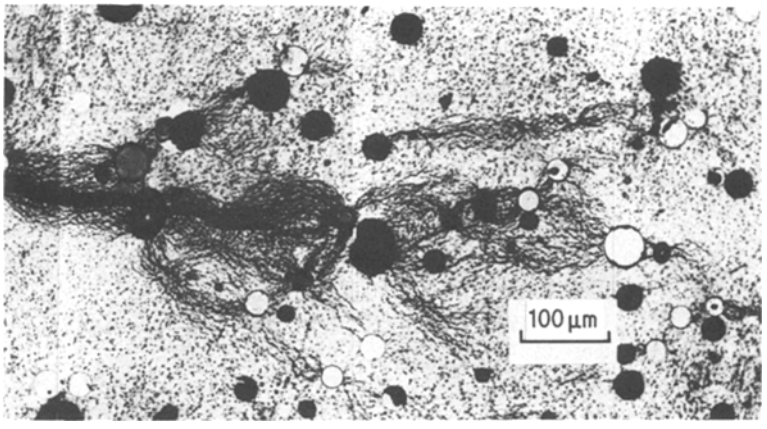

Figure 13 Optical reflection micrograph of crack growth in a hybrid-particulate composite. (v_f(glass) = 0.12; test temperature = 20° C.)

clear signs of plastically deformed material along the ridges. Recently Yee and Pearson [26] have obtained direct evidence for such shear yielding from optical microscopy studies of thin sections of rubber-modified epoxy viewed between cross polars. Localized shear bands are birefringent, and these were clearly visible running between rubber particles at an angle of about 45° to the maximum principal tensile stress, i.e. in the direction of the maximum shear stress. Finally it should be noted that, as in these previous studies, none of the distinctive fracture-surface features associated with a crazing mechanism was ever observed.

Now, whilst the rubbery particles undoubtedly act as the main initiation sites for shear yielding in the matrix, the glass particles may also induce some extra shear deformations. Evidence for this role of the glass particles is shown in Fig. 13, which is an optical micrograph of a crack propagating through a hybrid-particulate composite. The large dark holes are where glass particles have been removed during polishing of the sample. The light circular regions are glass particles, but some show dark arcs at the poles where debonding has apparently occurred ahead of the crack tip. The rubbery particles appear as very small dark particles. It may be seen that many fine black lines connect the rubbery particles in the vicinity of the crack, and tend to lie at an angle of about 45° to the maximum principal tensile stress (which is of course perpendicular to the crack direction) and therefore are indicative of plastic-shear bands. That they are indeed shear bands, rather than surface microcracks, was confirmed by examination of the specimens in the scanning electron microscope. The plastic-shear bands develop under constant volume deformation, which gives rise to furrows in the surface. These scatter the light in the optical microscope and the shear bands therefore appear as dark lines. The dark lines appear not only to be associated with the rubbery particles but also, to some extent, with the glass particles. Thus, the local stress concentrations introduced by the glass particles appear to assist in initiating shear deformations in the matrix. Hence the glass particles may increase the toughness by this mechanism as well as through the crack-pinning mechanism, and the former mechanism would be expected to be more significant at higher test temperatures when the yield stress of the matrix is relatively low.

4.2.2. Crack-tip blunting

A toughening mechanism which involves plastic-shear deformation highlights the importance of determining the yield behaviour of the composites [12] and of ascertaining the effect of such deformations on the extent of crack-tip blunting.

The value of the crack-opening displacement δ_{tc} obviously reflects the degree of crack-tip blunting, and values were therefore calculated using

$$\delta_{tc} = \frac{K_{Ic}^2}{E\sigma_{yt}} \quad (6)$$

where the respective values of K_{Ic}, E and σ_{yt} correspond to the test temperature of interest. Values of δ_{tc} are shown as a function of temperature for a hybrid-particulate composite in

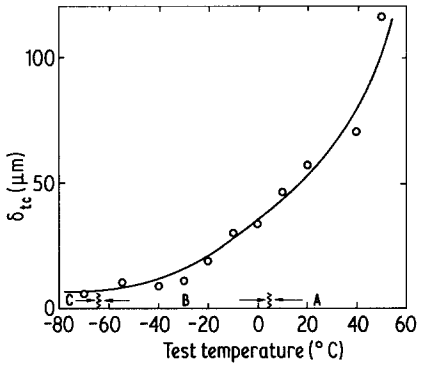

Figure 14 Crack opening displacement δ_{tc} at the onset of crack growth as a function of temperature for a hybrid-particulate composite (v_f(glass (silane)) = 0.12): Type C, stable brittle crack propagation; Type B, unstable brittle crack propagation; Type A, stable ductile propagation.

Fig. 14, and the types of crack propagation observed are also indicated. The dependence of δ_{tc} upon temperature and the transitions from Type C to Type B to Type A crack propagation with increasing temperature are typical of the behaviour of all the composites studied. The values of δ_{tc} increase with increasing temperature and this clearly demonstrates that the extent of localized plastic deformation and the associated crack-tip blunting increases steadily as the yield stress falls. This confirms the explanation offered for the crack-propagation behaviour in Section 3.1.1.

Now the relationship between fracture toughness, type of crack growth and yield behaviour may be expressed in a more quantitative manner by normalizing the measured values of the stress-intensity factor K_{Ic} at the onset of crack growth by K_{Ics}, i.e. the sharp crack-tip value. The ratio of K_{Ic}/K_{Ics} is shown plotted against the corresponding tensile yield stress σ_{yt} for the composites in Fig. 15. The results show a good correlation between toughness, the type of crack growth and the yield stress. This emphasizes the importance of localized plastic deformation in increasing the toughness, especially at higher temperatures.

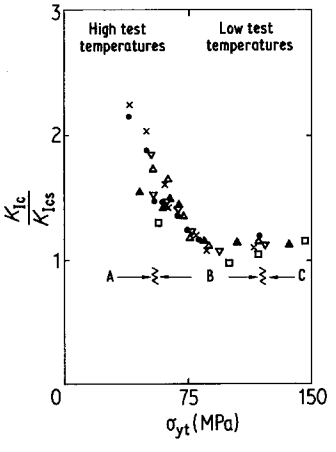

Figure 15 Relation between K_{Ic}/K_{Ics} ratio, tensile yield stress, σ_{ty} and type of crack growth for the hybrid-particulate composites containing silane-coated glass particles. Values of v_f(glass (silane)) as follows: (□) 0, (●) 0.036, (×) 0.085, (△) 0.012, (▽) 0.016, (▲) 0.27. Type A, stable ductile propagation; Type B, unstable brittle propagation; Type C, stable brittle propagation.

4.2.3. Theory and failure criterion

Previous theoretical analyses [15, 16, 27] have considered the stress distribution around a crack radius ϱ, and demonstrated that the ratio K_{Ic}/K_{Ics} may be expressed by

$$\frac{K_{Ic}}{K_{Ics}} = \frac{(1 + \varrho/2c)^{3/2}}{(1 + \varrho/c)} \quad (7)$$

where K_{Ics} is given by

$$K_{Ics} = \sigma_{tc} (2\pi c)^{1/2} \quad (8)$$

These relationships also indicate that the onset of crack growth is governed by a failure criterion based upon the attainment of a critical stress σ_{tc} acting over a certain distance c ahead of the crack tip. This expression has been found previously to represent a good quantitative description of the crack blunting mechanism and to provide a unique failure criterion, i.e. constant values of σ_{tc} and c are observed over a wide range of test conditions.

Values of K_{Ic}/K_{Ics} are plotted agains $\varrho^{1/2}$ for various particulate composites in Fig. 16. In accordance with previous work [15], values of the crack-tip radius ϱ at failure were deduced by assuming the value of ϱ to be equivalent to the crack-opening displacement δ_{tc}. The experimental data agree extremely well with the theoretical expression (Equation 7), establishing that the values of σ_{tc} and c are constant over the wide range of test temperatures employed. However, at high values of K_{Ic}/K_{Ics} (i.e. at high test temperatures) the experimental results fall somewhat below the theoretical curve in some instances. As discussed earlier, this may arise from debonding of the glass particles under these conditions. This explanation is supported by the observation that such discrepancies

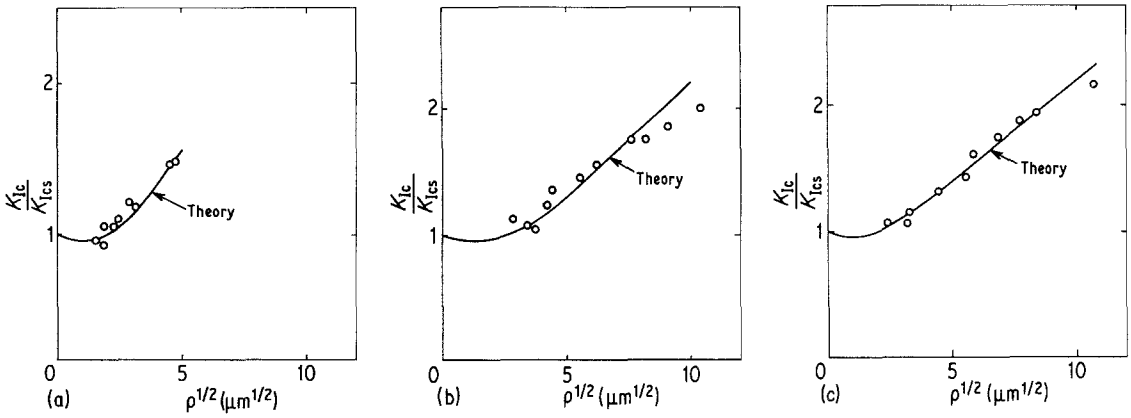

Figure 16 K_{Ic}/K_{Ics} ratio against $\rho^{1/2}$. Points experimental; full curve theoretical relation from Equation 7. (a) Glass-filled composite (v_f(glass) = 0.19); σ_{tc} = 470; c = 1.4 μm. (b) Hybrid-particulate composite (v_f(glass) = 0.12); σ_{tc} = 405 MPa, c = 2.8 μm. (c) Hybrid-particulate composite (v_f(glass (silane)) = 0.12); σ_{tc} = 425 MPa, c = 2.4 μm.

between experiment and theory occur more frequently for the uncoated-glass hybrid composites and at high values of v_f(glass); debonding is most likely to result under these conditions.

The experimental data, such as that shown in Fig. 16, together with Equations 7 and 8 yield values of σ_{tc} and c for each composite. The values of σ_{tc} typically lie between 400 and 600 MPa, with the values increasing with increasing v_f(glass) and being highest for the epoxy–glass composite. Thus, as noted previously [15], the values of σ_{tc} may be interpreted as a constrained yield stress and are generally lower for the tougher materials. The values of c are typically of the order of a few micrometres and are significantly higher for the tougher hybrid-particulate composites, but are almost independent of v_f(glass). Finally, since these parameters σ_{tc} and c are indeed constants for any given composition they do provide a unique failure criterion over the complete range of test temperature.

Thus, at low test temperature when crack pinning is a major mechanism, a single-parameter failure criterion is sufficient to describe the onset of crack growth. Furthermore, this mechanism appears to be strain-controlled, since a constant crack opening displacement is applicable. However, at higher test temperatures, crack tip blunting occurs due to extensive localized plastic deformation and a two-parameter failure criterion is now required. This mechanism appears to be stress-controlled, since it requires a critical stress level to be attained over a critical distance ahead of the crack.

5. Conclusions

The fracture behaviour of particulate-filled epoxy polymers has been examined and the following conclusions may be drawn:

1. Both rigid glass particles and rubbery particles may increase the toughness of a thermosetting epoxy polymer, but the latter type of dispersed phase has by far the greatest effect.

2. The addition of glass particles to an epoxy–rubber matrix, to give a hybrid-particulate composite, may significantly increase the toughness of the rubber-modified epoxy. At high test temperatures the value of K_{Ic} passes through a maximum as the volume fraction of glass particles is increased. This occurs at a v_f(glass) of about 0.1. This maximum is suggested to be a result of the glass particles debonding when higher volume fractions of glass are employed.

3. For the hybrid-particulate composites the maximum in the value of the fracture energy G_{Ic} at a v_f(glass) of about 0.1 is more pronounced, due to the modulus also increasing with increasing volume fraction of glass. At a value of v_f(glass) of about 0.1 the hybrid-particulate composites possess much higher fracture energies than the solely rubber-modified epoxy.

4. If the interfacial adhesion between the glass particles and the matrix is increased by using a reactive silane bonding agent, then the peak values of K_{Ic} (and G_{Ic}) for the hybrid-particulate composites are further raised. This observation obviously supports the above explanation for the K_{Ic} against v_f(glass) relation.

5. The glass particles mainly increase the

crack resistance by a crack-pinning mechanism. This represents a major contribution at the lowest test temperature, when a critical crack-opening displacement criterion may be applied.

6. The rubber particles increase the toughness by greatly enhancing the extent of plastic-shear deformations in the epoxy polymer at the crack tip, due to interactions between the stress field ahead of the crack and the rubbery particles. This leads to severe crack-tip blunting and can readily explain the temperature dependence of both the measured K_{Ic} values and the observed type of crack propagation. The crack-tip blunting mechanism may be described by a failure criterion which proposes that crack growth occurs when a critical stress is achieved over a critical distance ahead of the crack tip.

Acknowledgements

We would like to thank the Science Engineering Research Council for providing a research studentship for one of us (D.L.M.), and Mr D. Gilbert (Cambridge University) and Professor J. G. Williams (Imperial College) for helpful discussions and comments on various aspects of the work.

References

1. A. J. KINLOCH and R. J. YOUNG, "Fracture Behaviour of Polymers" (Applied Science, London, 1983) p. 421.
2. R. DRAKE and A. SIEBERT, *SAMPE Quart.* **6** (1975) 11.
3. J. N. SULTAN and F. T. McGARRY, *Polym. Eng. Sci.* **13** (1973) 29.
4. W. D. BASCOM, R. L. COTTINGHAM, R. L. JONES and P. PEYSER, *J. Appl. Polym. Sci.* **19** (1975) 2545.
5. A. J. KINLOCH, S. J. SHAW, D. A. TOD and D. L. HUNSTON, *Polymer* **24** (1983) 1341.
6. A. J. KINLOCH, S. J. SHAW and D. L. HUNSTON, *ibid.* **24** (1983) 1355.
7. F. F. LANGE and K. C. RADFORD, *J. Mater. Sci.* **6** (1971) 1197.
8. R. J. YOUNG and P. W. R. BEAUMONT, *ibid.* **12** (1977) 684.
9. A. C. MOLONEY, H. H. KAUSCH and H. R. STIEGER, *ibid.* **18** (1983) 208.
10. J. SPANOUDAKIS and R. J. YOUNG, *ibid.* **19** (1984) 473.
11. *Idem, ibid.* **19** (1984) 487.
12. R. J. YOUNG, D. MAXWELL and A. J. KINLOCH, *ibid.* **20** (1985).
13. J. G. WILLIAMS, "Fracture Mechanics of Polymers" (Ellis Horwood, Chichester, 1984) p. 46.
14. R. A. GLEDHILL, A. J. KINLOCH, S. YAMINI and R. J. YOUNG, *Polymer* **19** (1978) 574.
15. A. J. KINLOCH and J. G. WILLIAMS, *J. Mater. Sci.* **15** (1980) 987.
16. S. YAMINI and R. J. YOUNG, *ibid.* **15** (1980) 1823.
17. F. F. LANGE, *Phil. Mag.* **22** (1970) 983.
18. A. G. EVANS, *ibid.* **26** (1972) 1327.
19. D. G. GREEN, P. S. NICHOLSON and J. D. EMBRURY, *J. Mater. Sci.* **14** (1979) 1413.
20. *Idem, ibid.* **14** (1979) 1657.
21. A. K. KHAUND, U. D. KRISTIC and P. S. NICHOLSON, *ibid.* **12** (1977) 2269.
22. J. N. GOODIER, *J. Appl. Mech.* **1** (1933) 39.
23. B. D. AGARWAL and L. J. BROUTMAN, *Fibre Sci. Technol.* **7** (1974) 63.
24. A. J. KINLOCH, R. A. GLEDHILL and W. A. DUKES, "Adhesion Science Technology", edited by L. H. Lee (Plenum, New York, 1975) p. 597.
25. A. J. KINLOCH and S. J. SHAW, *J. Adhesion* **12** (1951) 59.
26. A. F. YEE and R. A. PEARSON, NASA Contractor Report 3718 (NASA, Langley, Virginia, USA, 1983).
27. J. G. WILLIAMS, "Stress Analysis of Polymers", 2nd Edn. (Ellis Horwood, Chichester, 1980) p. 350.

Received 16 November 1984
and accepted 23 January 1985